Reprinted from
ASLE TRANSACTIONS **8**, 296-305 (1965)
Academic Press Inc.
Printed in U.S.A.

The Load Capacity and Stability Characteristics of Hydrodynamic Grooved Journal Bearings

By G. G. HIRS[1]

The resultant pressure components and the stability characteristics of three grooved-bearing types have been determined for the case of near-center operation and non-compressible lubricants. The bearing parameters have been optimized in search of the best stability characteristics. The behavior at greater eccentricities and the use of gaseous lubricants have been dealt with in a qualitative way. Experiments are in agreement with the theory.

Nomenclature

x, y, z
$l, \varphi r$ = dimensional coordinates

λ, φ
X, Y = nondimensional coordinates

Dimensional Quantities

b = width
d = diameter
e = eccentricity
h = local film thickness
h_0 = film thickness on a dam in case of parallel surfaces, radial clearance
l = length
m = mass per unit of projected bearing area
p = pressure
Δp = pressure rise across length l
p_m = mean pressure per unit of projected bearing area
p_a = ambient pressure
r = radius
t = time
v = relative sliding speed
η = viscosity (dynamic)
ω = rotational speed (rad/sec)
M = (equivalent) mass
$\Phi_x, \Phi_y, \Phi_l, \Phi_{\varphi r}$ = volume flows across a unit length

All quantities appear in dimensionless numbers and so any consistent system of units can be used.

Dimensionless Quantities

α = lead angle
γ = groove width to wave length ratio
δ = greatest film thickness ratio in a groove and on a dam (parallel surfaces)
ϵ = e/h_0 = eccentricity vector
θ = angular displacement of eccentricity vector
$\dot{\theta}$ = whirl speed of eccentricity vector with respect to the bearing $\left(= \frac{1}{\omega}\frac{d\theta}{dt}\right)$
λ_0 = ratio of the axial length of a grooved part to the radius
λ_1 = ratio of the axial length of a plain part to the radius for asymmetrical patterns, or to the diameter for symmetrical patterns.
H = h/h_0 = ratio of local film thickness to minimum film thickness
H_1, H_2, etc. = mean values over one wavelength of functions of H
A to G, j, k = composite expressions of H_1, H_2, etc.
C_1, C_2, C_3, etc. = constants
$\frac{\Delta p \cdot h_0^2}{\eta v l}$ = pressure build-up number across grooved part at centric operation
$\Phi_\lambda = \frac{12\Phi l}{\omega r h_0}$ = dimensionless flow
$\Phi_\varphi = \frac{12\Phi_{\varphi r}}{\omega r h_0}$ = dimensionless flow
$N = \frac{\eta r^2}{m\omega h_0^3}$ = stability criterion
$P = \frac{p h_0^2}{\eta\omega r^2}$ = pressure number
$P_{11} = \frac{1}{\epsilon}\left(\frac{p_m h_0^2}{\eta\omega r^2}\right)_{11}$ = radial dimensionless mean pressure component of grooved journal bearing provided with a herringbone pattern, Fig. 1 (sliding)

Presented as an American Society of Lubrication Engineers paper at the Lubrication Conference held in Washington, D. C., October 13–16, 1964.

[1] Research Engineer, Institute T.N.O. for Mechanical Constructions, Delft, Holland.

$P_{12} = \frac{1}{\epsilon}\left(\frac{p_m h_0^2}{\eta\omega r^2}\right)_{12}$ = tangential component of same bearing (sliding)

$P_{13} = \frac{p_m h_0^2}{\eta \frac{d\epsilon}{dt} r^2}$ = radial component of same bearing (squeeze effect)

P_{21}, P_{22}, P_{23} = dimensionless mean pressure components of a journal bearing provided with a partly grooved, symmetrical pattern, Fig. 2

P_{31}, P_{32}, P_{33} = components of a bearing provided with a partly grooved, asymmetrical pattern, Fig. 3

$\frac{p_m h_0^2}{\eta\omega r^2}$ = load number $(= \epsilon [P_{11}^2 + P_{12}^2]^{\frac{1}{2}})$

Introduction

The possibility of generating pressure by means of relatively moving, grooved surfaces has been first mentioned by Gümbel (*1*). The herringbone grooved journal bearing of Fig. 1 has been patented by Hagg (*2*); he has also presented a qualitative appraisal of this bearing type.

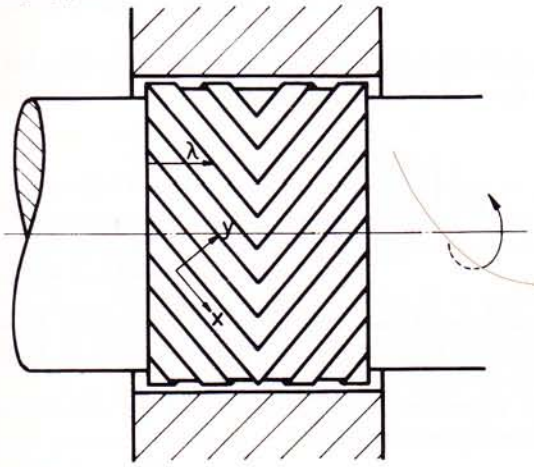

Fig. 1. Herringbone grooved journal bearing

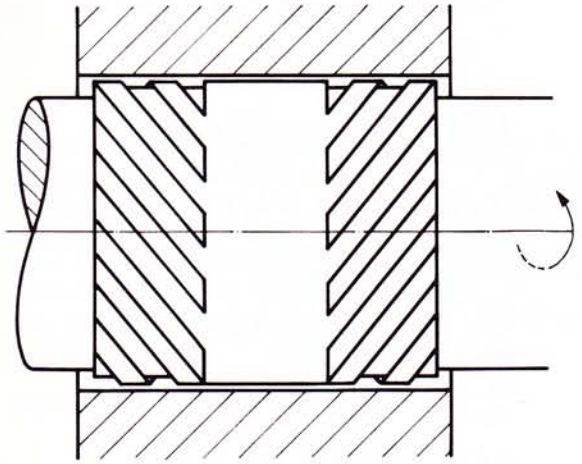

Fig. 2. Journal bearing, partly grooved; symmetrical pattern

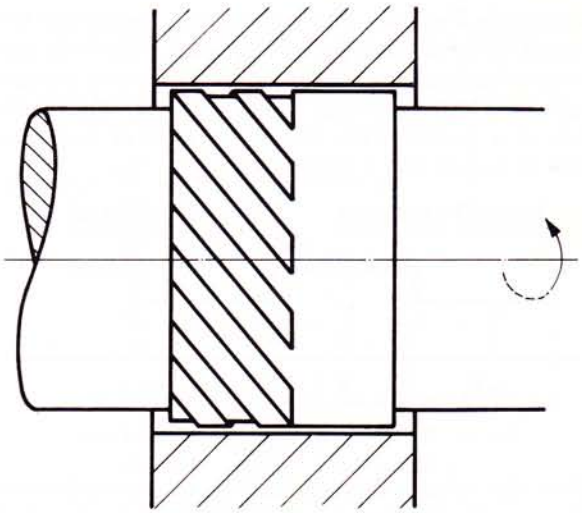

Fig. 3. Journal bearing, partly grooved; asymmetrical pattern

Two more groove patterns appear in Figs. 2 and 3. The asymmetrical pattern allows for a flow of coolant lubricant. The pressure distribution at centric operation has been determined by Whipple (*3*) and Boon and Tal (*4*) for somewhat different configurations.

Pressure distribution at eccentric operation

A cross section of the bearing appears in Fig. 4. The radial clearance (distance of dam and plain surface for the case of centric operation) has been denoted h_0. The ratio of the clearance in a groove and on a dam for the case of centric operation has been denoted δ. An eccentric operation (ϵh_0) gives a film profile around the

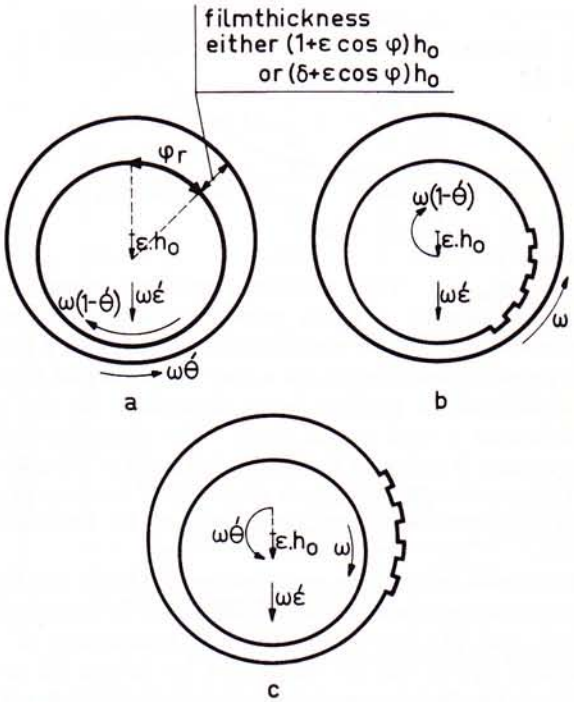

Fig. 4. Cross sections of grooved journal bearings

bearing as in Fig. 4a. The eccentricity vector has been assumed to be nonmoving in Fig. 4a. Figure 4b gives a nonmoving grooved journal; Fig. 4c gives a nonmoving grooved bearing lining. Figure 5 shows the relative width of a groove with respect to that of one wavelength of a dam and a groove.

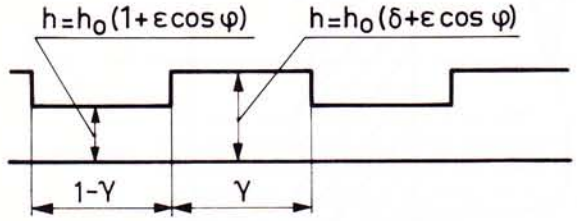

FIG. 5. Relative extension of groove and dam

Next the volume flows Φ_x and Φ_y, in groove direction and perpendicular thereto respectively, are going to be determined (see Fig. 1). The coordinate system x, y is connected to the eccentricity vector; it is not moving in Fig. 4a.

The groove direction can most easily be described by means of the herringbone groove pattern. It has been assumed that the herringbone (which can be regarded as a series of arrows) points in a clockwise direction. Either the bearing lining or the journal can be provided with grooves.

Equations [1] and [2] are the usual reductions of the Navier-Stokes formulas:

$$\frac{\partial p}{\partial x} = \eta \frac{\partial^2 v_x}{\partial z^2} \qquad [1]$$

$$\frac{\partial p}{\partial y} = \eta \frac{\partial^2 v_y}{\partial z^2}. \qquad [2]$$

The boundary conditions as in Fig. 4a result in Eq. [3] and [4].

$$\Phi_x = \frac{-1}{12\eta}\frac{\partial p}{\partial x} h^3 + \frac{1}{2}\omega(1 - 2\dot{\theta})h\, r \cos\alpha \qquad [3]$$

$$\Phi_y = \frac{-1}{12\eta}\frac{\partial p}{\partial y} h^3 - \frac{1}{2}\omega(1 - 2\dot{\theta})h\, r \sin\alpha \qquad [4]$$

The thickness h is either $(1 + \epsilon \cos\varphi)h_0$ or $(\delta + \epsilon\cos\varphi)h_0$. The pressure build-up consists of two components: a mean pressure distribution being dependent on the two coordinates x and y, and a wave-like pressure distribution (of a wavelength equal to that of a dam and a groove) being dependent on the two coordinates x and y and time. The time-dependent component is going to be eliminated in Eqs. [3] and [4].

The number of grooves is assumed to be very great. However, the flow is still assumed to be two-dimensional.

It follows from these assumptions that (1) the time-dependent component of the gradient $\partial p/\partial x$ is negligibly small, and (2) the time-dependent component of the gradient $\partial p/\partial y$ can be eliminated by taking its mean value, while making use of the fact that the flow across a dam and a groove is locally equal.

The first conclusion makes it possible to rewrite Eq. [3] and eliminate all time-dependent quantities.

$$(\Phi_x)_m = \frac{-1}{12\eta}\frac{\partial p}{\partial x}(h^3)_m + \frac{1}{2}\omega(1 - 2\dot{\theta})(h)_m r\cos\alpha. \qquad [5]$$

The subscript m denotes average values of the indicated quantities across a dam and a groove at place φ (see Fig. 5). The continuity of flow across a dam and a groove necessitates a separate analysis for a grooved bearing lining and a grooved journal.

The treatment is continued for the case of a grooved bearing lining. The law of continuity may not be applied to Φ_y (Eq. [4]) as a whole. Part of it $(+\omega\,\dot{\theta}\,h\,r\sin\alpha)$ is due to the motion of the grooved liner itself; however, the rest of it should be locally equal across a dam and a groove.

This feature can be expressed by introducing the mean pressure gradient in the y-direction:

$$\frac{-1}{12\eta}\left(\frac{\partial p}{\partial y}\right)_m \frac{1}{\left(\frac{1}{h^3}\right)_m} - \frac{1}{2}\omega r \frac{\left(\frac{1}{h^2}\right)_m}{\left(\frac{1}{h^3}\right)_m}\sin\alpha = \frac{-1}{12\eta}\frac{\partial p}{\partial y}h^3 - \frac{1}{2}\omega r\, h\sin\alpha \qquad [6]$$

Equation [6] has been inserted into Eq. [4]; Eq. [7] gives the mean value of the flow Φ_y.

$$(\Phi_y)_m = \frac{-1}{12\eta}\left(\frac{\partial p}{\partial y}\right)_m \frac{1}{\left(\frac{1}{h^3}\right)_m} - \frac{1}{2}\omega r \frac{\left(\frac{1}{h^2}\right)_m}{\left(\frac{1}{h^3}\right)_m}\mathrm{r}\sin\alpha + \omega\dot{\theta}(h)_m\, r\sin\alpha \qquad [7]$$

Equations [8] and [9] show the transition to a dimensionless form and the transformation to λ and φ coordinates (see Figs. 1 and 4a).

The transformation formulas and the dimensionless numbers appear below:

$$\Phi_{\varphi r} = (\Phi_x)_m\cos\alpha - (\Phi_y)_m\sin\alpha$$

$$\Phi_l = (\Phi_x)_m\sin\alpha + (\Phi_y)_m\cos\alpha$$

$$\frac{\partial p}{\partial x} = \frac{\partial p}{\partial l}\sin\alpha + \frac{\partial p}{r\partial\varphi}\cos\alpha$$

$$\left(\frac{\partial p}{\partial y}\right)_m = \frac{\partial p}{\partial l}\cos\alpha - \frac{\partial p}{r\partial\varphi}\sin\alpha$$

$$\Phi_\varphi = \frac{12\Phi_{\varphi r}}{\omega r h_0},\ \Phi_\lambda = \frac{12\Phi_l}{\omega r h_0},\ \lambda = \frac{l}{r},\ P = \frac{p h_0^2}{\eta\omega r^2} \text{ and } H = \frac{h}{h_0}$$

The dimensionless flows are:

$$\Phi_\lambda = -\frac{\partial P}{\partial\lambda}\left(H_3\sin^2\alpha + \frac{1}{H_{13}}\cos^2\alpha\right) - \frac{\partial P}{\partial\varphi}\left(H_3 - \frac{1}{H_{13}}\right)\sin\alpha\cos\alpha + 6\left(H_1 - \frac{H_{12}}{H_{13}}\right)\sin\alpha\cos\alpha \qquad [8]$$

$$\Phi_\varphi = -\frac{\partial P}{\partial \lambda}\left(H_3 - \frac{1}{H_{13}}\right)\sin\alpha\cos\alpha - \frac{\partial P}{\partial \varphi}\left(H_3\cos^2\alpha + \frac{1}{H_{13}}\sin^2\alpha\right) + 6\left(H_1\cos^2\alpha + \frac{H_{12}}{H_{13}}\sin^2\alpha\right) - 12\dot{\theta}H_1. \quad [9]$$

The dimensionless mean functions of the film thickness and a new way of writing have been specified in Eq. [10]. The quantity γ denotes the ratio of groove-width to wavelength (see Fig. 5). The differential equation has been expressed by Eq. [11].

$$\begin{aligned} H_1 &= (H)_m \\ &= (1-\gamma)(1+\epsilon\cos\varphi) + \gamma(\delta + \epsilon\cos\varphi) \\ H_2 &= (H^2)_m \\ &= (1-\gamma)(1+\epsilon\cos\varphi)^2 + \gamma(\delta+\epsilon\cos\varphi)^2 \\ H_{12} &= \left(\frac{1}{H^2}\right)_m \\ &= \frac{1-\gamma}{(1+\epsilon\cos\varphi)^2} + \frac{\gamma}{(\delta+\epsilon\cos\varphi)^2}, \text{ etc.} \end{aligned} \quad [10]$$

$$\frac{\partial \Phi_\lambda}{\partial \lambda} + \frac{\partial \Phi_\varphi}{\partial \varphi} = 0. \quad [11]$$

The squeeze effect as a result of a radial speed $\omega\dot{\epsilon} = d\epsilon/dt$ can be expressed by

$$\frac{\partial \Phi_\lambda}{\partial \lambda} + \frac{\partial \Phi_\varphi}{\partial \varphi} = 12\dot{\epsilon}\cos\varphi. \quad [12]$$

The above equations reduce to the plain journal bearing case and the well-known Reynolds equation by inserting $\delta = 1$ or $\gamma = 0$.

The above differential equation has been solved for the case of near-center operation. The series expansion of P is

$$P = P^0 + \epsilon P' + \epsilon^2 P'' + \epsilon^3 P''' + \ldots \quad [13]$$

The pressure-build-up P^0 follows from Eq. [8] for the case of $\epsilon = 0$;

$$\frac{12\Phi l}{\omega r h_0} = -\frac{\Delta p \cdot h_0^2}{\eta\omega r l}\left(H_3\sin^2\alpha + \frac{1}{H_{13}}\cos^2\alpha\right) + 6\left(H_1 - \frac{H_{12}}{H_{13}}\right)\sin\alpha\cos\alpha \quad [14]$$

The equation can be shown to be equivalent to that of Whipple (*3*) and Boon and Tal (*4*). It is zero for the case of symmetrical patterns. The first-order perturbation with respect to eccentricity has been carried out by differentiating the flows [8] and [9] with respect to eccentricity and inserting $\epsilon \to 0$.

The resulting Eqs. [15] and [16] lead to the differential equation as in [17].

$$\Phi'_\lambda = \frac{\partial P'}{\partial \lambda}\left(H_3\sin^2\alpha + \frac{1}{H_{13}}\cos^2\alpha\right) - \frac{\partial P'}{\partial \varphi}\left(H_3 - \frac{1}{H_{13}}\right)\sin\alpha\cos\alpha - 3P^0\left(H_2\sin^2\alpha + \frac{H_{14}}{H_{13}^2}\cos^2\alpha\right)\cos\varphi. + 18\left(1 - \frac{H_{12}H_{14}}{H_{13}^2}\right)\sin\alpha\cos\alpha\cos\varphi$$

$$-\Phi'_\lambda = A\frac{\partial P'}{\partial \lambda} + B\frac{\partial P'}{\partial \varphi} + D\cos\varphi \quad [15]$$

$$\Phi'_\varphi = -\frac{\partial P'}{\partial \lambda}\left(H_3 - \frac{1}{H_{13}}\right)\sin\alpha\cos\alpha - \frac{\partial P'}{\partial \varphi}\left(H_3\cos^2\alpha + \frac{1}{H_{13}}\sin^2\alpha\right) - 3P^0\left(H_2 - \frac{H_{14}}{H_{13}^2}\right)\sin\alpha\cos\alpha\cos\varphi - 18\left(1 - \frac{H_{12}H_{14}}{H_{13}^2}\right)\sin^2\alpha\cos\varphi + 6(1-2\dot{\theta})\cos\varphi$$

$$-\Phi'_\varphi = C\frac{\partial P'}{\partial \varphi} + B\frac{\partial P'}{\partial \lambda} + E\cos\varphi \quad [16]$$

$$\frac{\partial \Phi'_\lambda}{\partial \lambda} + \frac{\partial \Phi'_\varphi}{\partial \varphi} = 0 \quad [17]$$

Equation [18] shows the general solution to this differential equation; Eq. [19] shows the particular solution.

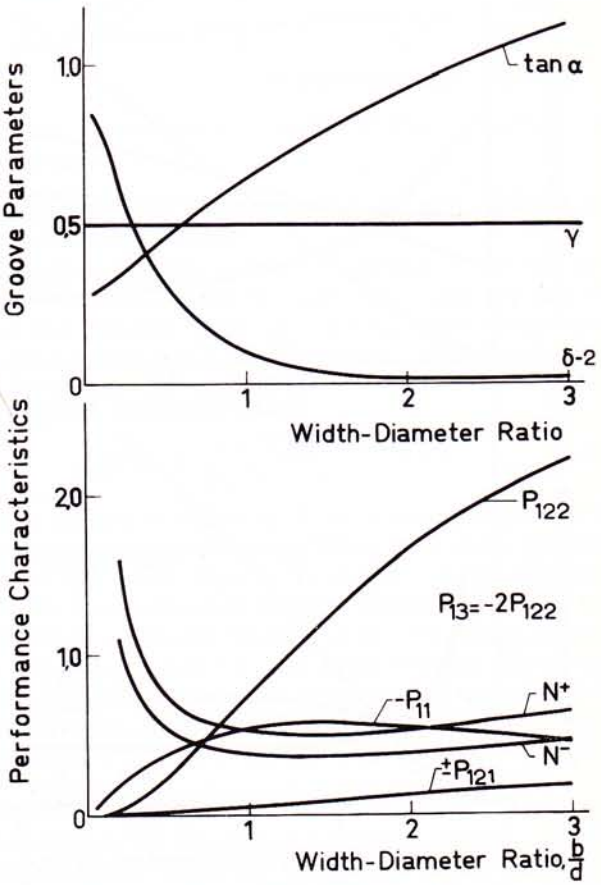

FIG. 6. Characteristics of the bearing of Fig. 1 (maximum $-P_{11}$).

The general solution to the squeeze effect is identical to [18]. The particular solution appears in [20].

$$P' = C_1(\cos\varphi\cos j\lambda\ \mathrm{CH}\ k\lambda + \sin\varphi\sin j\lambda\ \mathrm{CH}\ k\lambda) + C_2(\cos\varphi\cos j\lambda\ \mathrm{SH}\ k\lambda + \sin\varphi\sin j\lambda\ \mathrm{SH}\ k\lambda) + C_3(\cos\varphi\sin j\lambda\ \mathrm{CH}\ k\lambda - \sin\varphi\cos j\lambda\ \mathrm{CH}\ k\lambda) + C_4(\cos\varphi\sin j\lambda\ \mathrm{SH}\ k\lambda - \sin\varphi\cos j\lambda\ \mathrm{SH}\ k\lambda), \quad [18]$$

in which $j = B/A$ and $k = [(C/A) - (B/A)^2]^{1/2}$

$$P' = -\frac{E}{C}\sin\varphi \quad [19]$$

$$P' = -\frac{12}{C}\epsilon\cos\varphi. \quad [20]$$

The boundary conditions to these solutions are dependent on the actual groove patterns. The dimensionless pressure is zero at the free boundaries. The flow [15] or [8] is zero at a symmetrical axis of a grooved bearing. The flow [15] or [8] is locally continuous where grooved surfaces pass into plain surfaces.

Resultant Pressure Components and Stability

Equations [21] and [22] give the dimensionless resultant pressure components. The lengthy analytical work will not be presented here.

$$P_{11} = \frac{1}{2\lambda_0}\int_0^{\lambda_0}\int_0^{2\pi} P'\cos\varphi\, d\lambda\, d\varphi = \frac{1}{\epsilon}\left(\frac{p_m h_0^2}{\eta\omega r^2}\right)_{11} \quad [21]$$

$$P_{12} = \frac{1}{2\lambda_0}\int_0^{\lambda_0}\int_0^{2\pi} P'\sin\varphi\, d\lambda\, d\varphi = \frac{1}{\epsilon}\left(\frac{p_m h_0^2}{\eta\omega r^2}\right)_{12}. \quad [22]$$

The main result of this work is the appearance of a resultant pressure component P_{11}, P_{21}, or P_{31} opposing the eccentricity vector and securing the possibility of a stable operation at near-center operation. This component is nonexistent for the case of plain journal bearings. The restoring resultant pressure components have been subjected to a process optimization: maximizing a continuous nonlinear function of up to 6 independent variables by a refined gradient technique [see Dickinson (5)].

The results appear in Figs. 6, 7, and 8 for the case of the groove patterns of Figs. 1, 2, and 3, respectively. It has been shown that the restoring component of Fig. 2 is the greatest one possible: $P_{21} = -0.6866$ for

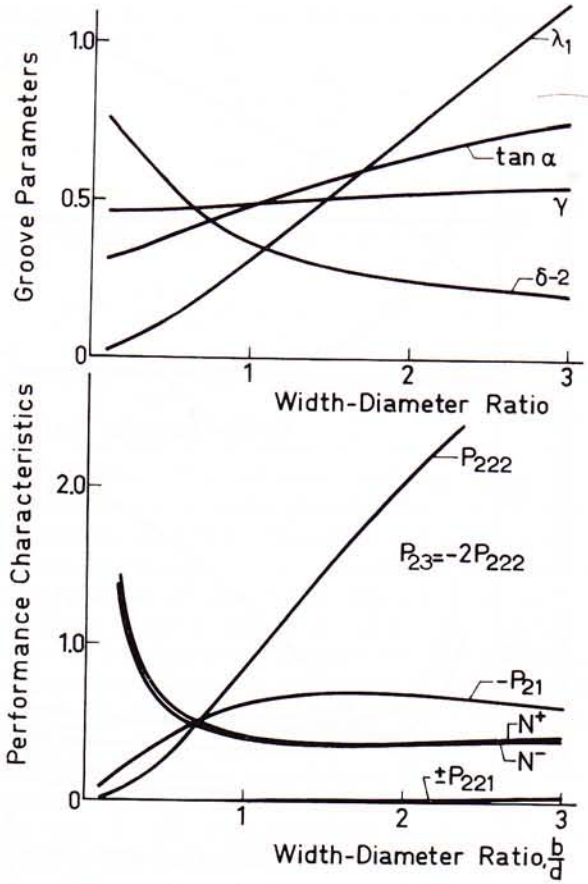

FIG. 7. Characteristics of the bearing of Fig. 2 (maximum $-P_{21}$).

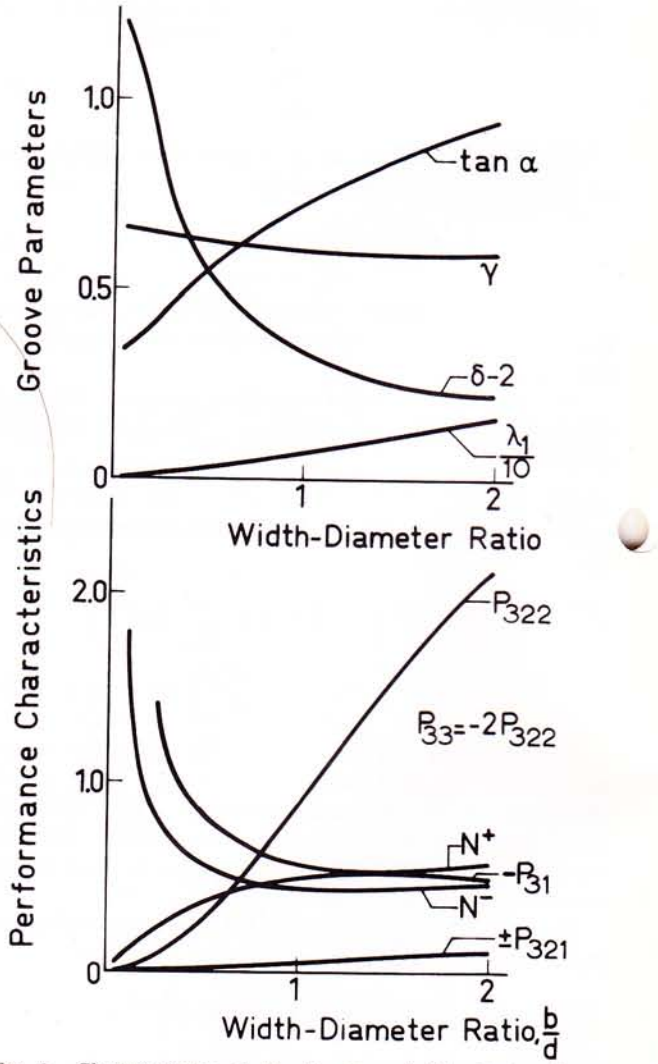

FIG. 8. Characteristics of the bearing of Fig. 3 (maximum $-P_{31}$).

the case of $\gamma = 0.558$, $\delta = 2.15 \tan \alpha = 0.677$, $b/d = 1.78$, $\lambda_1 = 0.553$.

The other resultant pressure components have been determined for the case of the relevant optimum groove parameters. The pressure component perpendicular to the eccentricity vector (P_{12}, P_{22}, and P_{32}) has been split as in Eq. [23].

$$P_{12} = P_{121}(\alpha, \gamma, \delta, \lambda) + (1 - 2\dot{\theta})P_{122}(\alpha, \gamma, \delta, \lambda). \quad [23]$$

The first part is positive for the case of a grooved bearing lining and is negative for a grooved journal if the lead angle has been chosen in such a way that P_{11} opposes the eccentricity vector. The second part P_{122} is half as great as the squeeze effect (see Figs. 6, 7, and 8); it is always positive.

The restoring force is of great importance in securing a stable operation. A quantitative appraisal is now possible at near-center operation. Plain bearings give anomalous results; they are not stable at near-center operation. Grooved journal bearings will be stable up to a maximum speed. Figure 4 is the starting point of the determination of the stability characteristics. The theory will be restricted to that of rigid shafts.

The mass distribution can be accounted for by fixing an equivalent point-mass to the geometric center of the journal in Fig. 4. The shaft is assumed to be perfectly balanced in this way. Next the circular coordinates of Fig. 4 are transformed into rectangular ones in Fig. 9. The resultant pressure components have also been inserted. The dynamic behavior in the two directions is given in dimensionless form:

$$X'' - P_{13}NX' - P_{11}NX = -(P_{121} + P_{122})NY \quad [24]$$

$$Y'' - P_{13}NY' - P_{11}NY = +(P_{121} + P_{122})NX. \quad [25]$$

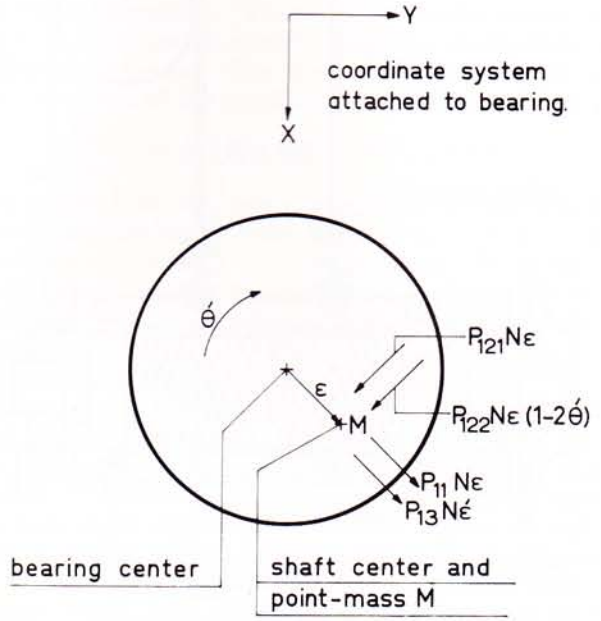

FIG. 9. Dynamic behavior of grooved journal bearing

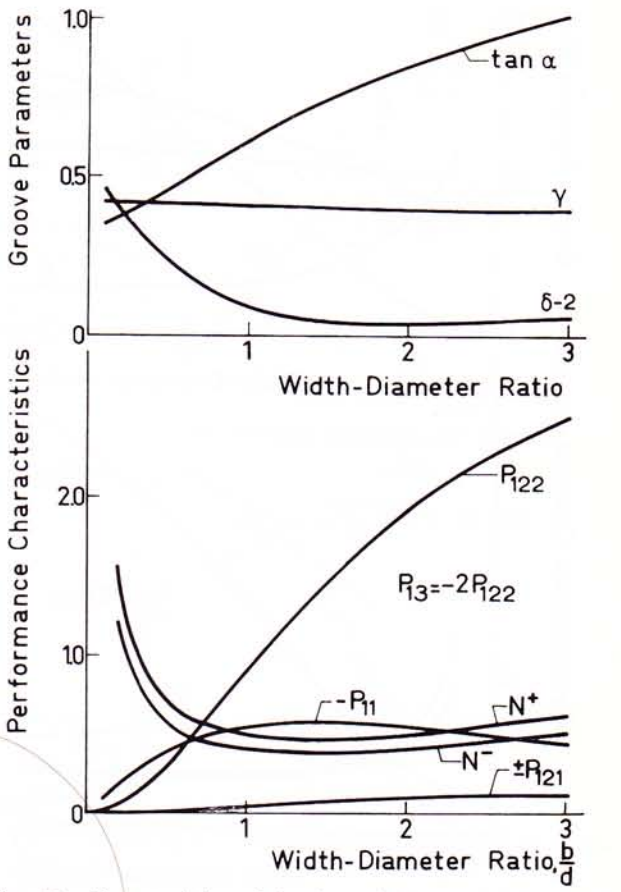

FIG. 10. Characteristics of bearing of Fig. 1 (minimum of $N+$).

The superscripts denote derivations with respect to dimensionless time (ωt).

The dimensionless number N appears in the nomenclature; it incorporates the equivalent mass per unit of projected bearing area (m) among other quantities. Routh's criterion (6) can be applied. Stable solutions to expressions [24] and [25] evolve if the criterion [26] is satisfied.

$$N > \frac{-1}{P_{11}} \left(\frac{P_{121} + P_{122}}{P_{13}} \right)^2. \quad [26]$$

The minimum values of N have been computed for the case of a grooved bearing lining (N^+) and a grooved journal (N^-) (see Figs. 6, 7, and 8). Next, criterion [26] has been subjected to the process-optimization for the case of a grooved bearing lining; the results appear in Figs. 10, 11, and 12. No great changes have been made apparent in this way; the restoring force is somewhat smaller, and the first part of the component perpendicular to the eccentricity vector [23] has been made very small.

Criterion [26] has also been subjected to process-optimization for the case of a grooved journal. There exist solutions where the component perpendicular to the eccentricity vector [23] is zero at $\dot{\theta} = 0$. Equations [24] and [25] reduce to a simple mass-spring-damp-

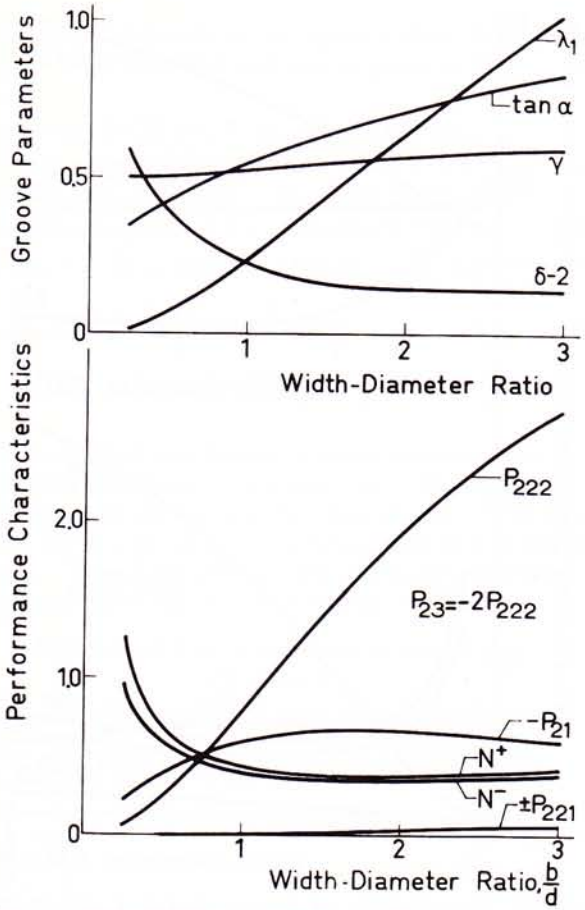

FIG. 11. Characteristics of bearing of Fig. 2 (minimum of $N+$).

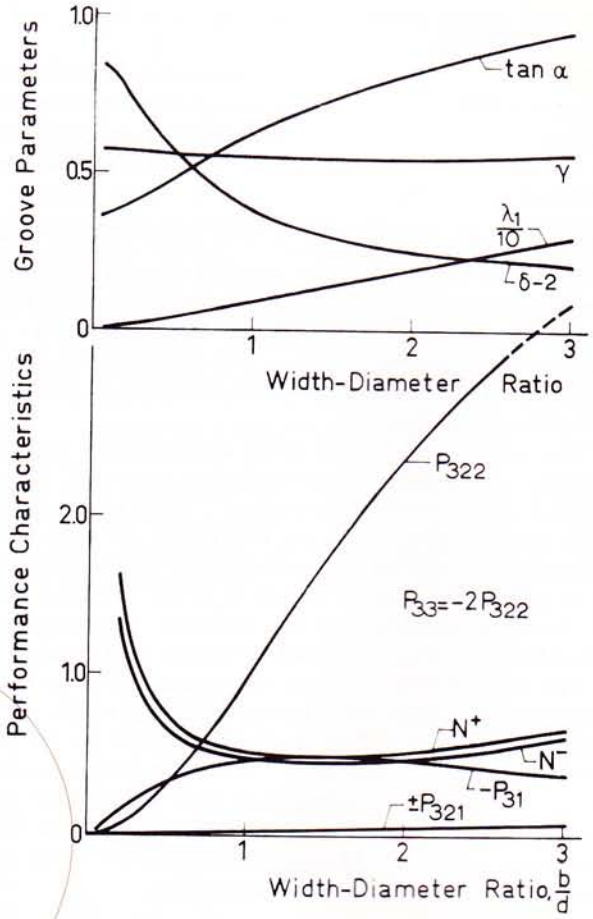

FIG. 12. Characteristics of bearing of Fig. 3 (minimum of $N+$).

ing system, which is always stable. These solutions are not of importance to bearing design, however. The load capacity is about ten times smaller than that of Figs. 6, 7, 8, 10, 11, and 12. Much better stability characteristics at reasonably great load numbers have not yet been found.

Experiments

The experimental apparatus appears in Fig. 13. A turbine-driven shaft on two ball bearings is provided with two herringbone groove patterns. The loose bearing shell can be loaded by means of strings over two pulleys. Springs of a very low stiffness are mounted in the strings in order to isolate the dynamic behavior of the loose shell. The attitude of the shell with regard to the journal can be measured by means of four sets of inductive pick-ups. The experimental groove parameters are not the optimized ones of the preceding treatment; the parameters have been inserted into the relevant formulas and numerical quantities have been obtained for P_{11}, P_{121}, P_{122}, and N. Theory and experiment are compared in Fig. 14. All bearing parameters have been made apparent. Figure 14a shows eccentricity versus the dimensionless load number. Two measuring series

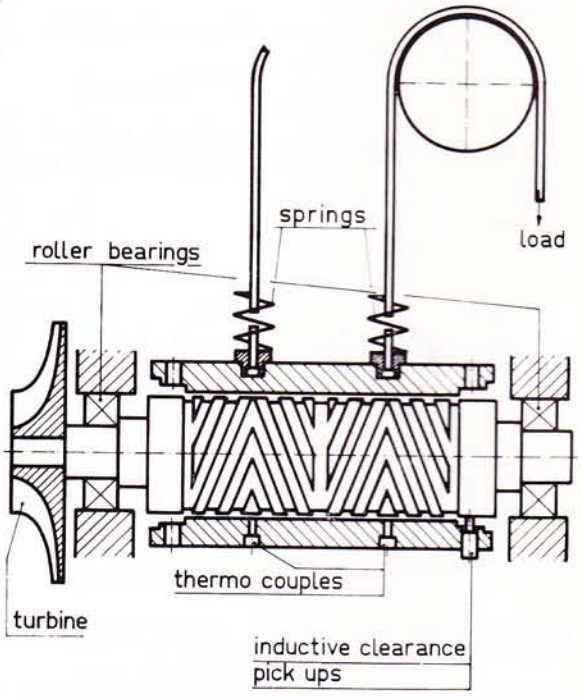

FIG. 13. Grooved journal bearing test apparatus

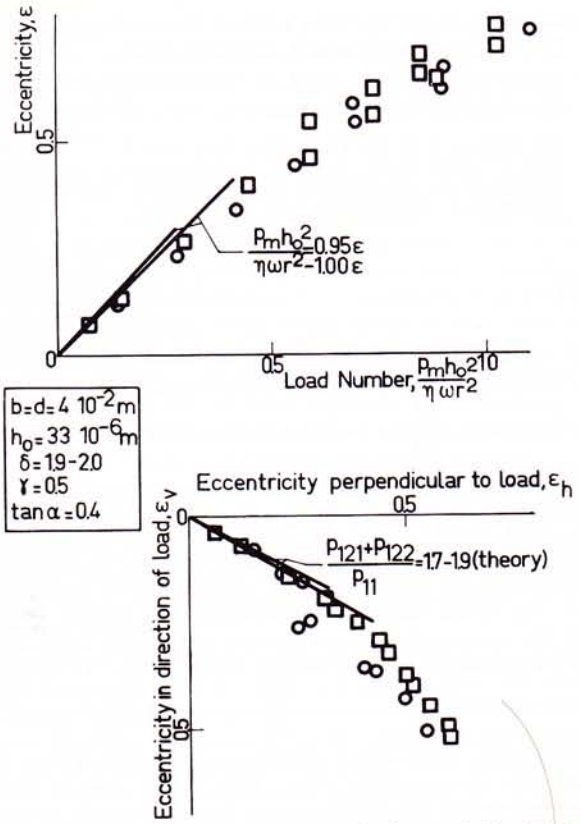

FIG. 14. Theoretical and experimental characteristics. □ 3024 rpm (air); ○ 80 rpm (oil).

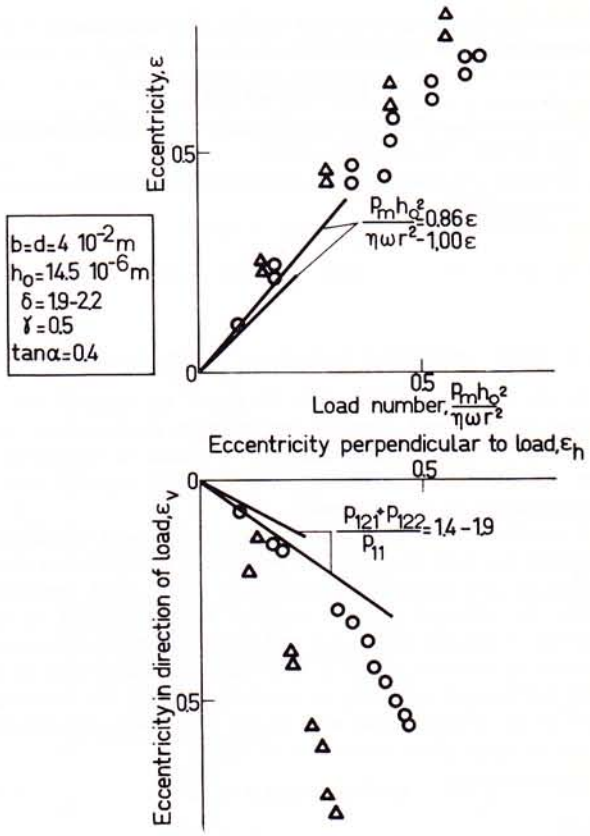

FIG. 15. Theoretical and experimental characteristics. ○ 5600 rpm ($\eta\omega r^2/p_a h_0^2 \sim 0.21$); △ 20,000 rpm ($\eta\omega r^2/p_a h_0^2 \sim 0.8$).

have been plotted, and they coincide. The first series accounts for low-viscosity oil lubrication at a very low speed; the second series accounts for air lubrication in a region where compressibility will not be of influence ($\eta\omega r^2/p_a h_0^2 \sim 0.03$). Figure 14b shows the attitude of the liner with regard to the journal; the load is in the vertical direction. Theoretical lines also appear in Fig. 14. The lines are straight because of the limitation to first-order terms. The theoretical load number is the vector sum of the resultant pressure components

$$\frac{p_m h_0^2}{\eta \omega r^2} = \epsilon[P_{11}^2 + (P_{121} + P_{122})^2]^{1/2}$$

It follows from the comparison between theory and experiment that higher-order terms of eccentricity give a positive contribution to the load number (Fig. 14a). It also follows that higher-order terms result in a greater displacement in the direction of load and a smaller displacement perpendicular thereto (see Fig. 14b).

Figure 15 shows the influence of compressibility in a grooved journal bearing. The influence can be shown to be smaller than in plain journal bearings. This feature is attributed to the pumping-in action of the grooves. Theoretical lines (noncompressible) have also been made apparent. Two lines appear in each graph, and they account for the scatter in the parameter δ. It is rather difficult to manufacture grooves with a constant depth of the present nominal value of 6×10^{-4} inch.

A comparison with theoretical and experimental values of the stability criterion N will not be given here. The experimental number is about the same magnitude as the theoretical one ($N^- \sim 0.5$) for the bearing of Fig. 15; the half-speed whirl started at 21,000–22,000 rpm. Other experiments are also in agreement with the theory. The scatter of results on stability will always be great, however, because of the many variables involved. An additional difficulty to interpretation in this experiment is the predominant occurrence of conical whirl; the theory accounts for cylindrical whirl.

It has been observed that the stability improves for the case of a loading to the bearing shell, and so higher-order terms of eccentricity seem to result in still lower values of the stability criterion. The bearing of Fig. 15 started to whirl at 30,000 rpm at an eccentricity ($\epsilon \sim 0.7$).

Conclusion

Grooved journal bearings have good and predictable stability characteristics. They can be stable at centric and near-center operation; plain journal bearings are not stable for that case.

ACKNOWLEDGMENTS

This work is part of a program on grooved bearings and seals at The Institute T.N.O. for Mechanical Constructions, Delft.

The author thanks Professor H. Blok of Delft University of

Technology for his interest and advice. He also thanks J. P. J. Lamers and J. de Vries for their mathematical aid.

REFERENCES

1. GUMBEL, L., "Reibung und Schmierung im Maschinenbau," pp. 80–82. Krayn, Berlin, 1925.
2. HAGG, A. C., "Bearing." U. S. Patent 2,479,349 (patented August, 1949).
3. WHIPPLE, R. T. P., "The Inclined Groove Bearing," AERE T/R 622 (revised), Harwell, Berkshire, 1958.
4. BOON, E. F. and S. E. TAL, "Hydrodynamische Dichtung für rotierende Wellen," *Chem. Ing. Tech.* **31,** 202–212 (1959).
5. DICKINSON, J. R. D., *Trans. Eng. Inst. Can.* **2,** (1958).
6. ROUTH, E. J., "A Treatise on the Stability of a Given State of Motion." Macmillan, New York, 1877.

DISCUSSION

C. Y. CHOW (*Mechanical Technology, Inc., Latham, New York*):

As the author pointed out in his paper, the analysis and the results for the load capacity and stability characteristics were based on an incompressible lubricant. It would be interesting to find the effect on the stability and the load capacity due to compressibility of the lubricant.

A stability criterion for journal bearings having a compressible lubricant has been developed by Pan (*A1*). It requires an examination of the bearing performance at those whirl frequencies where the attitude angle ϕ becomes zero. According to this criterion, if the derivative of ϕ with respect to whirl frequency is negative at the point where $\phi = 0$, then the critical mass of the rotor for onset of instability is found by equating the centrifugal force of the whirling rotor mass to the radial force of a bearing, $W \cos \phi$, at the point where $\phi = 0$, i.e.,

$$(gbDm_0)e(\omega_3)_0^2 = W \qquad [A1]$$

where

$(\omega_3)_0$ = whirl frequency at which $\phi = 0$
g = gravitational constant
m_0 = critical mass of rotor per unit projected area, at $\phi = 0$
e = eccentricity of bearing
D = diameter of bearing
b = length of bearing

Any mass larger than the critical mass is unstable under the above stated conditions. Thus, for a stable system, the rotor mass must be less than the critical mass m_0 in Eq. [*A1*], i.e.,

$$2\pi\overline{\omega}^2 / \left(\frac{\cos\phi}{S\varepsilon}\right) \leqslant \frac{\eta r^2}{m_0(\omega_1 + \omega_2)h_0^3} = N \qquad [A2]$$

where

$\overline{\omega} = (\omega_3)_0/(\omega_1 + \omega_2)$
ω_1 = angular speed of the smooth member of a groove bearing
ω_2 = angular speed of the grooved member of a grooved bearing

$$S = \frac{\eta(\omega_1 + \omega_2)\, bD}{2\pi W}\left(\frac{r}{h_0}\right)^2$$

$\varepsilon = e/h_0$ = eccentricity ratio
p_a = ambient pressure, psia

$$\Lambda = \text{compressibility number} = \frac{6\eta(\omega_1 + \omega_2)}{p_a}\left(\frac{r}{h_0}\right)^2$$

To compare the predicted stability of a compressible grooved bearing with the results obtained by the author for an incompressible bearing, we can use the analytical results obtained by Vohr and the discussor (*A2*) for the radial load and attitude angle of a whirling, fully grooved journal bearing at $\Lambda = 50$. From Figs. 13 and 14 of Reference (*A2*), the case of a smooth member rotating, the attitude angle ϕ for a bearing at $\Lambda = 50$ is zero at $\overline{\omega} = 1.22$. $\frac{\partial\phi}{\partial\overline{\omega}}$ is negative at this point and the value of $\frac{\cos\phi}{\varepsilon S}$ (dimensionless radial load) is 1.6. Substituting this into Eq. [*A2*] yields $N = 5.8$. Comparing this with the valu $N^+ = 0.51$ from Fig. 6 of the author's paper, we see that th critical mass for the bearing at $\Lambda = 50$ is about ten times less than the critical mass for the incompressible bearing operating with the same speed, lubricant viscosity and bearing configuration.

For the case of grooved member rotating, Figs. 13 and 14 of Reference (*A2*) gives $\phi = 0$, $\frac{\partial\phi}{\partial\overline{\omega}} < 0$ and $\frac{\cos\phi}{\varepsilon S} = 1.6$ at $\overline{\omega} = -0.22$. This yields $N = 0.19$ compared with $N^- = 0.385$ from Hirs' incompressible result. Thus, in the case of grooved member rotating, the critical mass at $\Lambda = 50$ is about twice that for the incompressible bearing.

The above numerical results illustrate two significant findings concerning the effect of compressibility on the stability of grooved journal bearings. First, compressibility has a very significant effect on the critical mass of the grooved journal bearing and, second, the critical mass of a compressible grooved journal bearing depends very strongly on whether the smooth or grooved member is rotating, the latter being the more stable situation.

As a closing word on stability, it should be mentioned that the stability criteria developed by Pan, when applied to the incompressible case, yields the same results as the Routh-Horowirz criteria used by the author.

As far as the groove geometry at the optimized radial load o stiffness under steady-state is concerned, the influence owing to compressibility number Λ at $\Lambda = 50$ can be seen from Fig. 7, 9 and 11 of Reference (*A2*). It is seen that the groove height ratio and angle tend to be greater, for optimized load at $\Lambda = 50$, than those at $\Lambda = 0$. The optimum groove parameters at $\Lambda = 0$ for the bearing mentioned above are identical to the ones found by the author.

REFERENCES

A1. PAN, C. H. T., "Spectral Analysis of Gas Bearing Systems for Stability Studies." To be published.
A2. VOHR, J. H., and CHOW, C. Y., "Characteristics of Herringbone Grooved, Gas-Lubricated Journal Bearings," Paper No. 64-Lub-15, presented at the ASME-ASLE International Conference, Washington, D.C., October 13–16, 1964.

AUTHOR'S CLOSURE:

The author appreciates Chow's attempt at a comparison of the two independent studies on grooved journal bearings presented at the International Lubrication Conference.

It is no surprise to him that the paper by Vohr and Chow (*A2*) on load capacity will be followed by a paper by Pan (*A1*) on the stability characteristics of these bearings. Favorable and predictable stability will be a very important characteristic in future applications.

Chow sets an undue limit to the scope of the author's paper by suggesting that it provides no information on characteristics because of the compressibility of the lubricant. It was expected that the pumping-in action of the grooves would suppress compressibility effects to a great extent in the majority of anticipated applications with gas-lubrication. The experiments confirmed this hypothesis. The analysis incorporating compressibility could then be regarded as a further refinement and was postponed to a later date. More attention could be devoted to the theory based on incompressible fluids. The evolving, relatively simple formulas for load capacity and stability characteristics could be optimized in a wider range of (groove) parameters and groove patterns.

It is difficult to review the as yet unpublished theory by Pan as quoted by Chow. Equations [*A1*] and [*A2*] of the discussion are identical to Eq. [26] of the paper. The author knew that the conditions mentioned in the second paragraph of the discussion are necessary in order to arrive at the stability criterion. They do not suffice, however.

The pressure component(s) owing to squeezing in the direction of the eccentricity must be taken into account also. The bearing can not be stable for instance if the squeeze effect is absent. The squeeze effect can be accounted for by applying Routh's method as it has been done in the paper. The absence of an account of the squeeze effect in Chow's numerical determination of the stability at the extremely high compressibility number used in his paper is questionable because the conditions can no longer be regarded to be an extrapolation from incompressible flow theory. The dynamic behavior at small eccentricities can no longer be described by the linear Eqs. [24] and [25]. At high compressibility numbers such equations will contain non-linear elements even if a first-order perturbation with respect to eccentricity is applied. The whirl speed for instance will be one of the non-linear variables in some concealed form. A further linearization seems arbitrary as long as nobody knows whether whirl speeds in a great range are physically compatible in practice as initial disturbances. This feature can be illustrated by Figs. 13 and 14 of the paper by Vohr and Chow. Chow predicts that the speed at which the rotating grooved member will whirl is negative. Hydrodynamic theory predicts that it is positive. And so it must be zero at some or other magnitude of the influence of compressibility. From Pan's theory it follows that bearing will always be stable when operating at this magnitude, which is unlikely. It is far more probable that excessive eccentricities will be built up when the journal whirls at speeds in a region where the attitude angle, or the sine component of the bearing force, is zero or nearly so.

A stability theory of grooved gas journal bearings must account for the squeeze effect and the initial disturbances. This statement can be seen as the conclusion of the preceding paragraph. An earlier paragraph has implied that one need not be too anxious about it because the influence of compressibility is small in most applications. Stability can be extrapolated from incompressible flow theory and the concept, in which the radial-bearing force should exceed the centrifugal force at a whirl speed where the sine component of the bearing force is zero, is very useful there (although not sufficient in a complete theoretical treatment).

The properties of the wholly grooved bearing with optimum parameters at $\frac{b}{d} = 1$ (Fig. 6) are compared in Fig. *B1*. The compressible flow solution has been done after submission of the

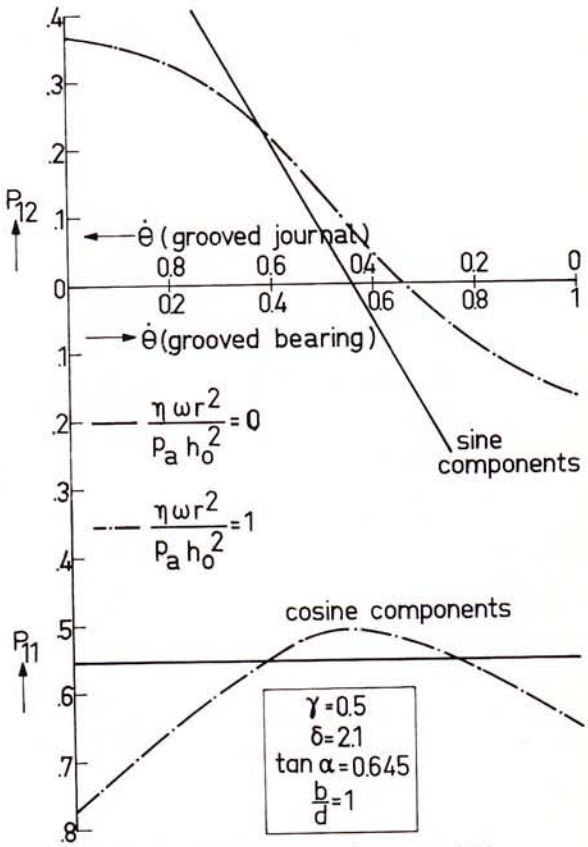

FIG. *B1*. The influence of compressibility

paper. The value of the compressibility number is about the maximum one to be found in practice under normal atmospheric pressure (or higher). The shift in whirl speeds where the sine component is zero is far less outspoken than in the case considered by Vohr and Chow. The cosine component is somewhat greater at whirl speeds zero and unity than for the case of incompressible flow. The load capacity is somewhat smaller at the higher influence of compressibility. The stability of the grooved journal is better and that of the grooved ~~journal~~ bearing is less favorable at the higher compressibility number. The shift in load capacity and stability is moderate.